Elastic scattering of 65 MeV positive and negative pions from nickel isotopes

B. Fick,* M. Blecher, K. Gotow, and D. Wright
Virginia Polytechnic Institute and State University, Blacksburg, Virginia 24061

R. L. Boudrie and R. L. Burman
Los Alamos National Laboratory, Los Alamos, New Mexico 87545

D. Mack, B. G. Ritchie,† and P. G. Roos
University of Maryland, College Park, Maryland 20742

J. A. Escalante, C. S. Mishra, B. M. Preedom, and C. S. Whisnant
University of South Carolina, Columbia, South Carolina 29208
(Received 31 January 1986)

Angular distributions of elastic differential cross sections were obtained at 65 MeV using positive and negative pions scattered from ^{58}Ni, ^{60}Ni, and ^{64}Ni. The data were compared to predictions using the Michigan State University optical potential. These predictions are not in good agreement with the data. The negative pion cross sections are more poorly described than the positive pion cross sections. The p-wave part of the potential is observed to be especially sensitive to this Coulomb-nuclear interference effect.

I. INTRODUCTION

If the full potential of the pion as a probe of nuclear structure is to be realized the basic pion-nucleus interaction mechanism must first be understood. It is particularly important to accomplish this at energies below resonance where the pion-nucleon interaction is weaker allowing the pion to penetrate deeper into the nucleus. The many-body nature of the problem has necessitated the use of optical potentials to describe the interaction. It is known that the potential must have a nonlocal part and that effects arising from true pion absorption, isospin, polarization of the nuclear medium, and the Pauli principle must be included.

The MSU potential,[1,2,3] a semiphenomenological optical potential which includes the effects listed above, has described much of the π^+ elastic scattering data at energies $\lesssim 50$ MeV. To extend the use of this potential to energies between 50 and 100 MeV would be of interest since this energy region represents the transition between low energy and resonant energy phenomena. It is also important to determine whether the potential adequately describes π^- elastic scattering and nuclear isospin effects. In this paper the results of pion elastic scattering from nickel isotopes and the comparison of the data with the MSU potential are reported.

II. EXPERIMENT

The experiment was performed using the Clamshell spectrometer on the low-energy pion channel (LEP) at the Clinton P. Anderson Meson Physics Facility (LAMPF). Specifically, the experiment consisted of the elastic scattering of positive and negative pions from ^{58}Ni, ^{60}Ni, and ^{64}Ni. These nickel isotopes were chosen because each is easily obtainable and has a first excited state which is more than 1 MeV removed from the ground state. The size of the expected isospin effect, $(N-Z)/A$, where N, Z, and A are the neutron, proton, and nucleon numbers, respectively, for these isotopes span the same range examined in previous experiments[4] on ^{13,14}C. Nickel, however, lies in the medium mass range which has not been well explored by pions at these energies. The targets were self-supporting foils of thickness 0.147, 0.151, and 0.146 g/cm^2. The beam spot on target was 0.5 cm vertically by 2.5 cm horizontally and the beam momentum spread was $\Delta p/p = 0.5\%$. The 65 MeV data was obtained for scattering angles between 30 and 110 deg.

The layout of the spectrometer magnet, scattered pion detection system, and beam monitor system is shown in Fig. 1. The clamshell magnet is a dipole with a nonuniform field produced by inclined pole faces. This design provides for a short (2 m) flight path and a large solid an-

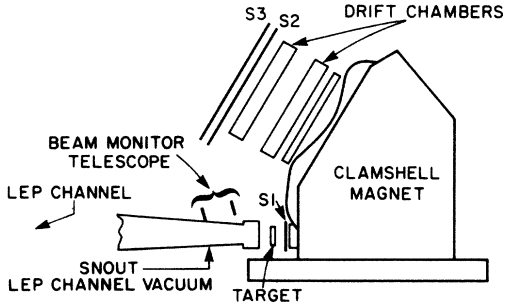

FIG. 1. The clamshell magnetic spectrometer system, S_1,S_2,S_3 are trigger scintillators. The relative beam monitor telescope is composed of scintillation counters.

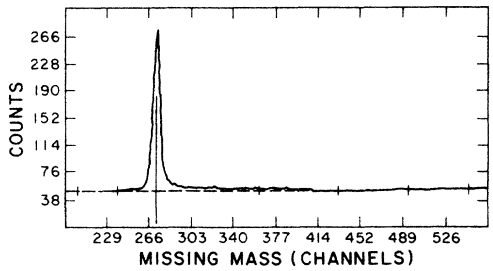

FIG. 2. Missing-mass histogram for π^- on ^{60}Ni at 30°. The bottom scale is 0.1 MeV per channel. A 50 count level has been added during processing.

gle (36 msr). Knowledge of the particle trajectory at the focal plane enables the determination of the trajectory at the target. The device has a momentum acceptance of ±30% and maximum acceptable momentum of 250 MeV/c. The energy resolution obtained in the present experiment with targets in air and scintillator $S1$ present to reduce background was 700 keV (FWHM).

The focal plane detector array consists of two drift chamber assemblies behind which are two scintillators, $S2$ and $S3$, with phototubes at each end. Each chamber assembly is capable of measuring the intersection point of a particle's path in two dimensions. They consist of two separate orthogonally oriented multiwire drift chambers each with an active area of 90 cm by 21 cm.[5] The left-right drift chamber ambiguity was resolved by cathode charge measurement[6] in order to minimize the number of wire planes and resultant multiple scattering.

The pion beam was monitored by using pairs of scintillation counters set to look at decay muons emitted by the beam at the exit of the LEP channel. These observe the π-μ decay phase space region for a small length of the beam. The number of coincident events is proportional to the number of pions in the beam.

Cross sections were obtained from the data by fitting the elastic peaks in the missing-mass spectra with a line shape extracted from the data. A typical missing-mass spectrum, obtained at forward angles, is shown in Fig. 2. A reference line shape was selected from the data in accordance with three criteria: (1) there must be no visible excited states in the chosen spectrum; (2) the chosen peak must contain a statistically significant number of counts; (3) the extent of the low energy tail associated with the peak must be discernable.

Normalization of the differential cross sections was achieved by taking scattering data from CH_2 and ^{12}C targets at scattering angles of 50, 55, 60, 70, 90, and 100 deg. A missing-mass histogram for hydrogen was produced by subtracting the suitably scaled ^{12}C histogram bin by bin from the corresponding CH_2 histogram. A normalization factor, $(f\cdot\epsilon\cdot\Delta\Omega)$, was obtained by comparing the cross sections calculated with the above yields to cross sections derived from published phase shifts[7] (errors in the phase shifts were not included). Here, f is a constant which relates the number of counts in the beam monitor to the in-

TABLE I. Differential cross sections for π^+-nickel elastic scattering. Scattering angles and cross sections are in units of degrees and (mb/sr), respectively. Errors shown are relative errors. The absolute normalization error is 6%.

^{58}Ni (π^+,π^+)			^{60}Ni (π^+,π^+)			^{64}Ni (π^+,π^+)		
$\theta_{c.m.}$	$\frac{d\sigma}{d\Omega}\Big\|_{c.m.}$	$\Delta\frac{d\sigma}{d\Omega}\Big\|_{c.m.}$	$\theta_{c.m.}$	$\frac{d\sigma}{d\Omega}\Big\|_{c.m.}$	$\Delta\frac{d\sigma}{d\Omega}\Big\|_{c.m.}$	$\theta_{c.m.}$	$\frac{d\sigma}{d\Omega}\Big\|_{c.m.}$	$\Delta\frac{d\sigma}{d\Omega}\Big\|_{c.m.}$
30.1	145.0	4.0	30.1	161.0	4.0	30.1	189.0	3.0
36.1	98.2	7.7	40.1	61.4	1.1	40.1	66.9	1.2
40.1	61.6	1.6	46.2	33.3	2.2	46.1	35.1	2.6
46.2	34.0	1.7	50.2	14.2	1.0	50.2	14.8	1.2
50.2	14.6	0.6	55.2	10.2	0.2	55.2	8.8	0.2
55.2	10.7	0.3	60.2	6.5	0.4	60.2	8.0	0.5
60.2	8.7	0.6	65.2	6.8	0.2	65.2	6.9	0.2
65.2	7.1	0.2	70.2	5.6	0.3	70.2	7.0	0.3
70.2	6.0	0.3	78.3	3.0	0.5	78.3	3.0	0.5
81.4	2.8	0.3	80.6	2.6	0.3	80.6	2.6	0.3
84.2	1.4	0.2	82.9	1.7	0.3	82.9	1.8	0.4
86.5	1.1	0.1	83.4	1.4	0.2	83.6	1.1	0.2
87.9	0.64	0.11	85.7	0.86	0.11	85.9	0.60	0.09
91.2	0.25	+0.06, −0.18	87.9	0.36	0.09	88.2	0.37	0.10
93.5	0.25	+0.09, −0.18	88.6	0.25	+0.08, −0.18	89.3	0.27	+0.06, −0.21
95.0	0.35	+0.08, −0.27	90.9	0.18	+0.05, −0.13	91.6	0.17	+0.05, −0.12
97.3	0.77	0.10	93.2	0.23	+0.06, −0.17	93.9	0.28	+0.10, −0.21
99.3	1.1	0.2	94.3	0.48	0.09	95.2	0.43	0.09
99.6	1.4	0.3	96.6	0.83	0.15	97.4	1.0	0.1
101.6	1.5	0.2	98.9	1.4	0.3	99.2	1.7	0.3
103.9	2.7	0.5	99.2	1.6	0.2	99.7	1.9	0.3
110.2	4.8	0.2	101.5	1.8	0.2	101.5	2.0	0.2
			103.8	2.2	0.4	103.8	3.2	0.6
			110.2	4.3	0.2	110.2	5.0	0.3

TABLE II. Differential cross sections for π^--nickel elastic scattering at 65 MeV. Scattering angles and cross sections are in units of degrees and (mb/sr), respectively. Errors shown are relative errors. The absolute normalization error is 6%.

^{58}Ni (π^-,π^-)			^{60}Ni (π^-,π^-)			^{64}Ni (π^-,π^-)		
$\theta_{c.m.}$	$\frac{d\sigma}{d\Omega}\Big\|_{c.m.}$	$\Delta\frac{d\sigma}{d\Omega}\Big\|_{c.m.}$	$\theta_{c.m.}$	$\frac{d\sigma}{d\Omega}\Big\|_{c.m.}$	$\Delta\frac{d\sigma}{d\Omega}\Big\|_{c.m.}$	$\theta_{c.m.}$	$\frac{d\sigma}{d\Omega}\Big\|_{c.m.}$	$\Delta\frac{d\sigma}{d\Omega}\Big\|_{c.m.}$
30.1	395.0	30.0	30.1	375.0	22.0	30.1	454.0	27.0
40.1	90.2	7.0	40.1	87.6	7.0	40.1	91.7	8.3
50.2	39.5	2.2	50.2	34.7	2.1	50.2	45.4	2.6
60.2	32.6	1.4	60.2	28.4	1.3	60.2	36.3	1.6
70.2	15.8	0.8	70.2	13.5	0.7	70.2	15.4	0.9
75.2	4.9	0.4	75.2	3.7	0.4	75.2	4.2	0.4
81.1	3.2	0.2	80.1	2.5	0.2	80.9	3.1	0.2
83.1	1.6	0.3	83.1	1.0	0.3	84.1	1.7	0.3
85.4	0.92	0.1	85.4	0.65	0.1	86.4	1.6	0.2
87.7	0.79	0.2	87.7	1.0	0.2	87.7	3.4	0.7
90.9	2.3	0.1	90.2	2.2	0.1	91.5	3.6	0.2
96.2	2.9	0.2	95.9	3.9	0.2	96.2	5.4	0.2
101.5	4.9	0.2	100.5	5.2	0.3	101.3	7.0	0.3
110.2	5.7	0.3	110.2	5.9	0.3	110.2	6.5	0.4

cident pion flux, ϵ is a constant which contains the overall efficiency, and $\Delta\Omega$ is the solid angle. The value obtained for the normalization factor is 0.087. The standard deviation of the set of data points, 6.0%, is taken as the absolute normalization error.

The angular distributions were corrected for finite solid angle effects. Phase shift fits to the uncorrected laboratory cross sections were used to obtain first and second derivatives of the cross sections with respect to angle; these derivatives were then used in analytic calculations of the finite solid angle corrections. The effect of the correction is a reduction of the cross section at very forward angles and a deepening of the minima.

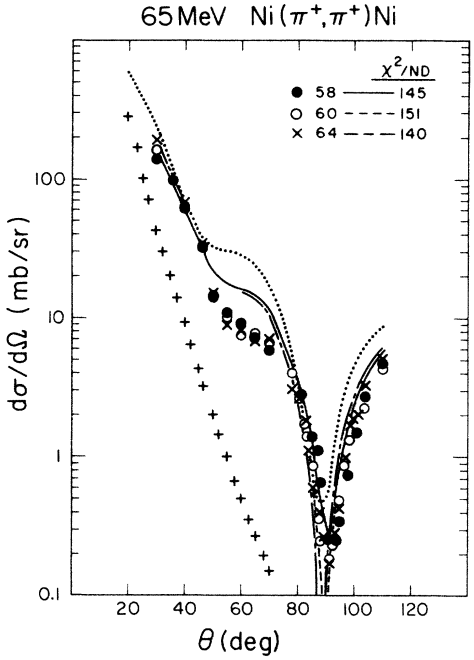

FIG. 3. Elastic differential cross sections for π^+ scattering on ^{58}Ni, ^{60}Ni, and ^{64}Ni at 65 MeV. The solid, dashed, and dash-dot curves are predictions of the MSU potential using the parameters of Table III. Also listed are the chi-squared per degree of freedom between experimental and predicted cross sections. The dotted curve is the prediction of the MSU potential for ^{58}Ni with the Coulomb effect removed, ^{58}Ni$(\pi^0,\pi^0)^{58}$Ni, while the cross curve is for just the Coulomb effect.

III. DATA

The differential cross sections obtained are listed in Tables I and II and displayed, with error bars suppressed for clarity, in Figs. 3 and 4. The errors quoted for the cross sections do not include the 6% absolute normalization error.

The most obvious characteristic of the 65 MeV π^+ elastic cross sections is the similarity between them for ^{58}Ni, ^{60}Ni, and ^{64}Ni. The second characteristic of note concerning the π^+ cross sections is their very deep and narrow diffraction minima.

The 65 MeV π^- cross sections have diffraction minima less deep than the corresponding π^+ diffraction minima. This situation of deep minima for π^+ and shallower minima for π^- is the reverse of that observed at 50 MeV.[8] Also, in the π^- data one sees that past a scattering angle of 90° the data for the different isotopes begin to differ from each other. This isotopic spin difference dependence is most pronounced between the angles of 85° and 105°.

IV. ANALYSIS OF THE DATA

An optical potential used in the analysis of low energy data is the MSU potential, in particular Eq. (1) of Ref. 3. This potential represents a compromise between fits to pionic atom data and fits to elastic scattering data. However, above 50 MeV incident pion energy this model begins to break down, possibly because it is too far from pionic atom energies and too close to the 3-3 resonance. It was therefore decided to reduce the pionic atom influ-

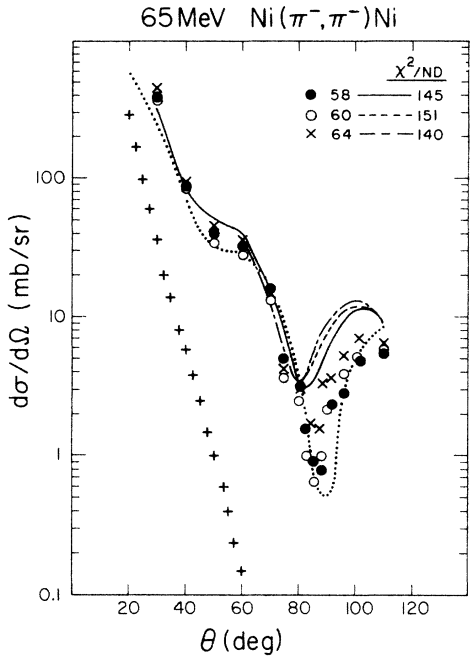

FIG. 4. Elastic differential cross sections for π^- scattering on ^{58}Ni, ^{60}Ni, and ^{64}Ni at 65 MeV. The solid, dashed, and dash-dot curves are predictions of the MSU potential using the parameters of Table III. Also listed are the chi-squared per degree of freedom between experimental and predicted cross sections. The dotted curve is the prediction of the MSU potential for ^{58}Ni with the Coulomb effect removed, ^{58}Ni$(\pi^0,\pi^0)^{58}$Ni, while the cross curve is for just the Coulomb effect.

ence by employing the scattering potential of Eq. (5) of Ref. 1.

The MSU potential is semiphenomenological in that only a few of its parameters need to be found by fitting to data. The parameter set chosen for the analysis of the data is a modified version of what Ref. 3 calls parameter set E, where parameters were obtained from π-N phase shifts, fitting to pionic atom level shifts and widths and to 50 MeV π^+ scattering data. To analyze the 65 MeV data, parameter set E was modified as follows. The single particle parameters were obtained from pion-nucleon phase shifts. The isovector absorption parameters were assumed to be zero. Thus, all the isospin dependence of the potential rests with the terms in the single particle parameters. The isoscalar absorption parameters were linearly extrapolated to 65 MeV from parameter set E. The parameters used in this analysis are listed in Table III.

The charge and matter densities were obtained from electron scattering data.[9] The neutron density was assumed to have the same shape as the proton density, which was found sufficient to describe 50 MeV scattering[8] from Ni and 50 MeV scattering[10] from ^{14}C.

The MSU potential containing the parameters previously described was used to predict the 65 MeV differential cross sections shown in Figs. 3 and 4. The π^+ calculation agreed well with the data except at the s-p wave interference minima at $\simeq 50°$. It successfully predicted the deep and narrow first diffraction minima at $\simeq 90°$ and the virtual lack of isospin dependence. The π^- prediction is a different story. The predicted values of the differential cross sections differed noticeably from the data at all but the most forward angles. The predicted diffraction minima were shallower and occurred at a lower scattering angle than the data. The data and the calculation agreed that an isospin dependence exists for angles past these minima and they agreed on the relative ordering of the dependence. In these calculations all the isospin dependence is contained in the single particle terms. Thus the observed ordering in the π^- case is just what is expected due to the increase in potential strength arising from increasing nucleon number.

TABLE III. 65 MeV MSU potential parameters used in the analysis. The Pauli factor, $Q=0.43$, is included in the imaginary parts of the single particle parameters.

b_0 (fm) $= -0.074+0.0095i$
b_1 (fm) $= -0.122-.0005i$
c_0 (fm^3) $=0.76+0.0645i$
c_1 (fm^3) $=0.48+0.031i$
$\lambda=1.4$
B_0 (fm^4) $= -0.028+0.07i$
C_0 (fm^6) $=0.38+0.46i$

It should be noted that because the MSU potential has zero range, the parameters used here produce a singular wave equation. This singularity is encountered if the real p-wave strength exceeds unity at some radius.[11] At the radius where this part of the potential equals one, an anomalous absorptive dipole layer appears. Even if the imaginary part of the potential is set to zero, the reaction cross section will not vanish. The presence of this singularity for all three isotopes indicates that the simple modification of set E parameters requires improvement especially if one insists on a zero range potential.

In an attempt to rectify the problems discussed above, variations were made in the absorption parameters. Good fits to the data could be obtained only if the resulting potential for π^+ differed from the π^- potential in the real p-wave isoscalar term. The differences between π^+ and π^- in the diffraction minima are due to Coulomb-nuclear interference; particularly Coulomb interference with the p-wave part of the potential. The need for two potentials to reproduce the data in the region of the diffraction minima points out the sensitivity to this portion of the potential this interference affords.

To further illustrate the cancellations occurring here, the pure Coulomb and pure nuclear cross sections for ^{58}Ni are also shown in Figs. 3 and 4. In the region of the minima, the destructive (constructive) interference for π^+ (π^-) is quite evident. Similar results are also found at 50 MeV. Here the Coulomb interaction is stronger and the nuclear interaction is weaker resulting in deeper minima for π^-.

These parameter variations, however, did not change the singular nature of the potential. For this reason the physics content of such parameter variations is unclear and the fitted values of the parameters are not reported.

V. SUMMARY

Elastic scattering data for 65 MeV pions scattered from ^{58,60,64}Ni were compared to predictions made by the MSU optical potential. The predictions and the data were not found to be in good agreement.

Coulomb-nuclear interference is seen to be important especially at positions of minima in the cross sections. The treatment of this effect in the MSU potential may be responsible for the fact that the π^- cross sections are more poorly described than are those of π^+. The deep diffraction minima in Ni and the fact that they are shallower for π^+ than for π^- at 50 MeV but the reverse at 65 MeV, should provide a stringent test for the proper description of this effect.

ACKNOWLEDGMENTS

The authors thank the staff of LAMPF for their support during the experiment. Special thanks are due to L. Attencio for his aid in constructing the focal plane drift chambers. This work was supported by grants from the United States National Science Foundation (Virginia Polytechnic Institute and State University, University of South Carolina, and the University of Maryland) and by the United States Department of Energy (Los Alamos National Laboratory).

---

*Present address: University of Utah, Salt Lake City, UT 84112.

†Present address: Arizona State University, Tempe, AZ 85287.

[1]K. Stricker, H. McMannus, and J. A. Carr, Phys. Rev. C **19**, 929 (1979).

[2]K. Stricker, H. McMannus, and J. A. Carr, Phys. Rev. C **22**, 2043 (1980).

[3]J. A. Carr, H. McMannus, and K. Stricker-Bauer, Phys. Rev. C **25**, 952 (1981).

[4]M. Blecher, K. Gotow, R. L. Burman, M. V. Hynes, M. J. Leitch, N. S. Chant, L. Rees, P. G. Roos, F. E. Bertrand, E. E. Gross, F. E. Obenshain, T. P. Sjoreen, G. S. Blanpied, B. M. Preedom, and B. G. Ritchie, Phys. Rev. C **28**, 2033 (1983).

[5]L. G. Atencio, J. F. Amann, R. L. Boudrie and C. L. Morris, Nucl. Instrum. Methods **187**, Nos. 2 and 3, 381 (1981).

[6]A. Breskin, G. Charpak, and F. Sauli, Nucl. Instrum. Methods **151**, 473 (1978).

[7]R. A. Arndt and L. D. Roper, Centre for Analysis of Particle Scattering, VPI&SU, Blackburg, VA 24061, 1985.

[8](a) C. S. Mishra, G. S. Blanpied, J. A. Escalante, B. M. Preedom, M. Blecher, K. Gotow, W. Burger, R. L. Burman, M. V. Hynes, and G. Chiangaru, Proceedings of the X International Conference on Particles and Nuclei, Heidelberg, Germany, 1984, edited by B. Povh and G. Z. Putlitz (unpublished). (b) C. S. Mishra *et al.* (unpublished).

[9]C. W. DeJager, H. DeVries, and C. DeVries, At. Data Nucl. Data Tables, **14**, 479 (1974).

[10]C. S. Mishra, B. M. Preedom, B. G. Ritchie, R. S. Moore, M. Blecher, K. Gotow, R. L. Burman, M. V. Hynes, E. Piasetzky, N. S. Chant, P. G. Roos, F. E. Bertrand, T. Sjoreen, F. E. Obenshain, and E. E. Grass, Phys. Rev. C **32**, 995 (1985).

[11]T. E. O. Erickson and F. Myhrer, Phys. Lett. **74B**, 163 (1978).